PCCP

PAPER

View Article Online
View Journal | View Issue

Cite this: *Phys. Chem. Chem. Phys.*, 2016, **18**, 792

Size-dependent strain and surface energies of gold nanoclusters†

S. Ali,[a] V. S. Myasnichenko[b] and E. C. Neyts*[a]

Received 12th October 2015,
Accepted 18th November 2015

DOI: 10.1039/c5cp06153a

www.rsc.org/pccp

Gold nanocluster properties exhibit unique size-dependence. In this contribution, we employ reactive molecular dynamics simulations to calculate the size- and temperature-dependent surface energies, strain energies and atomic displacements for icosahedral, cuboctahedral, truncated octahedral and decahedral Au-nanoclusters. The calculations demonstrate that the surface energy decreases with increasing cluster size at 0 K but increases with size at higher temperatures. The calculated melting curves as a function of cluster size demonstrate the Gibbs–Thomson effect. Atomic displacements and strain are found to strongly depend on the cluster size and both are found to increase with increasing cluster size. These results are of importance for understanding the size- and temperature-dependent surface processes on gold nanoclusters.

1. Introduction

It is well known that nanoclusters (NCs) have different physical and chemical properties compared to their bulk counterparts, due to their large surface-to-volume ratio, specific geometries and electronic structure.[1] Additionally, particular structural relaxation and surface reconstruction phenomena of nanoclusters further greatly influence their electronic and optical properties.[2,3]

Gold nanoclusters in particular display unique electronic, optical and catalytic properties. Control over these properties allows their use in a variety of applications, including *e.g.* nanolithography,[4] nanophotonics,[5,6] catalysis[7–9] and biomedicine.[10] Hence, it is of great importance to understand the structure and stability of gold nanoclusters.

An important descriptor of the solid surface with respect to its reactivity is the surface energy.[11,12] Previously, it has been reported in many studies that modification of the surface energy can lead to a change in the particle shape.[13–15] This in turn affects both the kinetics and thermodynamics of processes taking place at the particle surface.[16,17] While the surface tension of liquids has been understood for over 100 years, the surface energy of solids is not nearly as well understood, despite its paramount importance in catalysis, crystal growth, colloidal behavior, sintering, fracture, and essentially every other surface-mediated process.[18] Most of the experimental surface energy studies[19–26] available for solids are doubtful to at least some extent and are in poor agreement with each other as well[13,21,27] and often include uncertainties of unknown magnitude.[26] This makes the computational study of the surface energy very important. Furthermore, metal clusters exhibit unique size-dependent properties,[7,28–30] and surface energies of nanoclusters are often considered to be of prime importance for their catalytic activity.[31] It is therefore of interest to study the surface energy and closely related surface properties such as strain as a function of cluster size.

At the nanoscale, the most stable structures are the icosahedron, cuboctahedron and decahedron.[31,32] Ino *et al.* predicted that icosahedral Au clusters should be stable up to sizes of 40 000 atoms.[33,34] Previous studies proposed that geometries with {111} surfaces are highly stable and do not melt below the bulk melting temperature, in contrast to structures containing {100} and {110} surfaces.[34–36] In contrast to the icosahedron, however, both the cuboctahedron and the truncated octahedron show the fcc structure, and thus correspond to minimum energy structures for fcc metals such as gold.[37–39] Moreover, the stability of icosahedral clusters decreases significantly with increasing cluster size.[34,40–42]

Hence, for the smallest metallic clusters, the icosahedron is the most stable structure, but for larger clusters the cuboctahedron, truncated octahedron and decahedron are more stable.[31,32] Based on the second moment approximation tight binding calculations, Myshlyavtsev *et al.* found that for clusters containing 923 atoms or less the icosahedron is the most stable structure, while the stability crossing with the cuboctahedral structure was found for 561 atoms or less when using the quantum Sutton–Chen potential.[43] This energetic difference between icosahedra and cuboctahedra is generally attributed to balancing the higher

[a] *Research Group PLASMANT, Department of Chemistry, University of Antwerp, Universiteitsplein 1, 2610 Wilrijk-Antwerp, Belgium. E-mail: erik.neyts@uantwerpen.be; Fax: +32-3-265-23-43; Tel: +32-3-265-23-88*

[b] *Scientific Production Company "Katren", 4 Timakov st. Novosibirsk, 630060, Russia*

† Electronic supplementary information (ESI) available. See DOI: 10.1039/c5cp06153a

surface stability of the {111} facets of icosahedra against the elastic distortion induced by their five-fold symmetry. In smaller clusters, the surface stability dominates, favoring the icosahedral shape, while for larger clusters the elastic distortion dominates, favoring the fcc lattice. Typically, both cuboctahedra and icosahedra contract relative to the bulk atomic positions. With increasing size, this contraction vanishes for cuboctahedra, while it increases with increasing size for icosahedra.[44] The stability of different polyhedral geometries of the nanoclusters can be determined *e.g.* by calculating potential energies. For instance, Li *et al.* found that for very small Au nanoclusters the icosahedron is much more stable than Ino-decahedral and cuboctahedral structures. However, their calculations demonstrated that for larger clusters Ino-decahedral clusters are more stable.[31]

The effect of temperature, however, on the surface and strain energies remains an outstanding issue. Previously, surface energy calculations for a pure Au cluster containing 256 atoms at different temperatures reported an increase in surface energy with temperature.[45] Another study carried out to determine the size-dependence of surface energies for Au nanoparticles reported a decrease in surface energy against the cluster size.[13] Similar studies were also carried out for Ni,[12] Ag[2] and Al[46] nanoparticles which also indicated a decrease in surface energy with increasing cluster size. Many molecular dynamics studies were previously carried out to investigate the melting of Au nanoclusters, based on different interatomic potentials such as the Embedded-Atom Method potential,[47–51] the Sutton–Chen potential[52] and the many-body glue potential.[34] Similarly, there are many studies reporting on the melting behavior of *e.g.* clusters of Ag,[53] Cu,[54] Ni[55] and other metals[56,57] using molecular dynamics simulations.

Most of the above stated studies emphasize on the size-dependent melting behavior, rather than the size-dependent surface and strain energies of Au nanoclusters. So, we here report on surface energy calculations for icosahedral, cuboctahedral, truncated octahedral and decahedral gold nanoclusters in a wide range, containing 116 up to 6525 atoms. Since lattice strain can influence the surface energy and the relevant mechanical properties,[58] we also calculate the size dependence of the atomic displacements and associated strain.

2. Simulation model and method

Surface energies and strain of the Au-nanoclusters are calculated using classical molecular dynamics (MD) simulations. In a MD simulation, the time trajectories of all atoms in the system are followed through space by integrating the equations of motion. Forces are derived as the negative gradient from a suitable interatomic potential.

We here employ the standard Embedded Atom Method (EAM) potential[59,60] as implemented in the LAMMPS code[61,62] to describe the interatomic interactions. The temperature range investigated is 100 K–1300 K. Previously, the EAM potential has been used to successfully calculate the surface properties of gold nanoclusters[47–51] as well as for other metals.[2,55]

We consider 9 icosahedral and 9 decahedral clusters of different sizes (containing N = 147, 309, 561, 923, 1415, 2057, 2869, 3871 and 5083 Au atoms). Each icosahedral cluster has a full-closed surface consisting of 20 close-packed triangular faces corresponding to {111} faces in the crystal lattice. The clusters with these atomic/mass numbers are the so-called magic number clusters, which show an increased stability relative to non-magic number clusters.[31,63–66] Similarly, we also consider 5 cuboctahedra (containing N = 309, 923, 2057, 3871 and 6525 atoms) and 5 truncated octahedra (containing N = 116, 490, 1288, 2670 and 4796 atoms), where each cluster is cut from the fcc lattice. A graphical representation of these structures is provided in the ESI.†

The surface energy is calculated as[2,12,13,45]

$$E_{\text{surface}} = \frac{E_{\text{P,cluster}} - E_{\text{P,bulk}}}{A_{\text{cluster}}} \quad (1)$$

where $E_{\text{P,cluster}}$ is the potential energy of the cluster, $E_{\text{P,bulk}}$ is the potential energy of a bulk system containing the same number of atoms, and A_{cluster} is the total cluster surface area. To calculate the surface energy at 0 K, we minimized the structure using the congate gradient minimization method[67,68] with a force tolerance of 1.0×10^{-8} eV Å^{-1}. For the calculation of the surface energy at non-zero temperatures, MD simulations are carried out in the canonical ensemble. The temperature is controlled by the Nose–Hoover thermostat[69] employing a relaxation constant of 100 fs.

In all calculations, the time step was set to 1 fs and each system was equilibrated for 300 ps prior to analysis. The surface energies at finite temperatures were calculated based on average potential energies and cluster surface areas, averaging over the final 2000 snapshots of the simulation, corresponding to 2 ps using eqn (1). Cluster surface areas were calculated using the qhull code.[70,71] The structural evolution of the nanoclusters during the melting process is analyzed by means of the Ackland–Jones bond-angle method,[72] allowing assigning the crystal type (fcc, hpc or bcc) to each atom. The Ovito[73,74] software package is used for visualization.

3. Results and discussion

3.1. Size dependent surface energy of icosahedral gold nanoclusters

Since the surface of an icosahedron consists of {111} facets, while the surfaces of cuboctahedral, truncated octahedral and decahedral clusters are composed of both {111} and {100} facets, we first calculate the surface energy of these facets for an infinite surface. We find values of 0.79 J m^{-2} for the {111} facet which is in good agreement with the values in the range 0.72–0.80 J m^{-2} as calculated by Singh-Miller and Marzari,[75] Almora-Neyvis *et al.*,[76] Holec *et al.*[13] and Crljen *et al.*[77] using Density Functional Theory (DFT) and 0.79 J m^{-2} and 0.89 J m^{-2} as calculated by Keith *et al.*[78] using EAM and Modified Embedded Atom Method (MEAM) potentials, respectively, to be compared to an experimental value of 1.10–1.50 J m^{-2} for the {111} facet.[20,79,80]

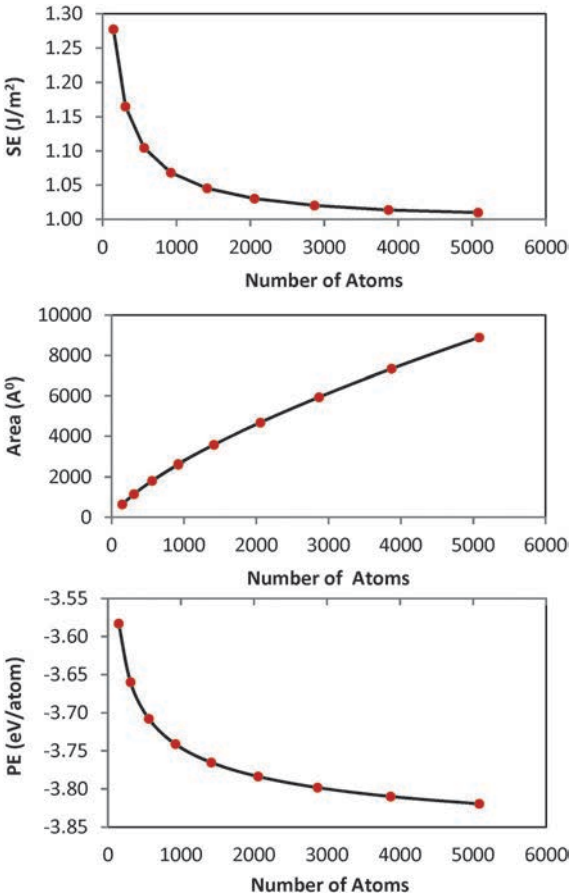

Fig. 1 Calculated surface energies (top panel), surface area (middle panel) and the potential energy per atom (bottom panel) for icosahedral clusters as a function of size.

Similarly, we find a value of 0.92 J m^{-2} for the {100} facet which is also in reasonable agreement with 0.88 J m^{-2} and 0.87 J m^{-2} as calculated by Almora-Neyvis *et al.*[76] and Holec *et al.*[13] using DFT, 1.04 J m^{-2} as calculated by Diao *et al.*[81] using the MEAM potential and 0.92 J m^{-2} and 1.08 J m^{-2} as calculated by Keith *et al.*[78] using EAM and MEAM potentials, respectively. While the EAM potential thus yields an absolute value for the surface energy too low to be compared to the experiment, as is also the case for the DFT calculations, the EAM potential correctly predicts the {111} facet to be the lower energy surface.

The calculated surface energies for the icosahedral gold nanoclusters as a function of size at 0 K are shown in Fig. 1 (top panel). Fig. 1 also shows the cluster surface area and the potential energy per atom for different icosahedral clusters (middle panel and bottom panel, respectively). It can be seen in Fig. 1 that the surface energy at 0 K decreases for increasing cluster size. This effect is due to the decrease in the surface-to-volume ratio for increasing particle size as shown in Fig. 2. Indeed, as the particle size becomes smaller, the potential energy per atom decreases (*i.e.* becomes more negative; see Fig. 1, bottom panel) due to the increasing fraction of under-coordinated surface atoms with lower cohesive energy. These results are in line

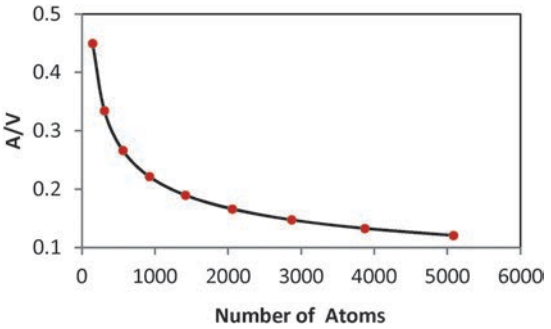

Fig. 2 Calculated surface to volume ratio for the icosahedral clusters as a function of size.

with literature results for surface energies of Ni[12] and Ag[2] nanoclusters. Note that the large surface-to-bulk ratio in nanoclusters is also (in part) responsible for their high chemical reactivity. Indeed, the large fraction of surface, edge and corner sites is in part responsible for an associated change in surface energy.[9,82]

Due to thermal expansion and thermal disorder, however, the surface area and surface energy of a nanocluster are naturally also a function of temperature. In Fig. 3, we show the calculated temperature dependence of the surface energy for icosahedral gold nanoclusters containing 561 and 3871 atoms, respectively, in the temperature range 0–1300 K. The figure shows a sharp increase in surface energy at 800 K and 900 K for the smaller and larger clusters, respectively, typical for signaling the onset of melting of the clusters. The increase in the onset temperature for melting for the larger cluster compared to the smaller cluster is in agreement with the Gibbs–Thomson effect. The observed trends are similar to earlier reports for melting Au[34,47–51] and other[53–57,83,84] nanoclusters.

Moreover, we also observe a strong increase in surface energy with increasing temperature for the larger cluster, which is larger than in the case of the smaller cluster. Thus, while the surface energy decreases with increasing cluster size at 0 K as shown above, it increases with increasing size at high temperatures. Indeed, the Au_{3871} cluster shows a surface energy of 1.810 J m^{-2} at 1300 K, to be compared with a lower surface energy of 1.464 J m^{-2} for the smaller Au_{561} cluster. Note that the crossing of the surface energies occurs near the melting interval of both clusters.

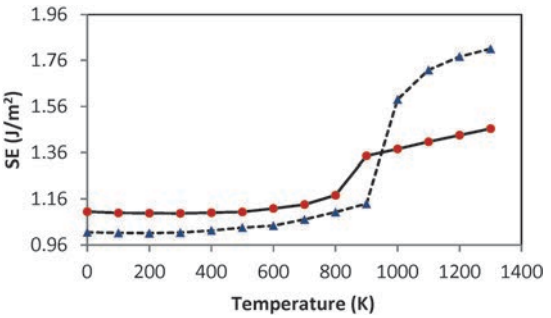

Fig. 3 A comparison of surface energies for the icosahedral clusters Au_{561} (red circles) and Au_{3871} (blue triangles) in the temperature range 0–1300 K.

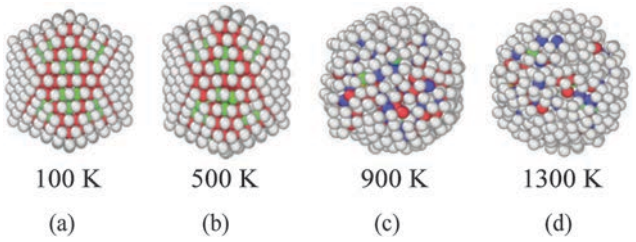

Fig. 4 Icosahedral structure of the Au_{561} cluster at (a) T = 100 K, (b) T = 500 K, (c) T = 900 K and (d) T = 1300 K. Green, red and blue represent fcc, hcp and amorphous cores, respectively, while white shows other undefined coordinations.

Thus, below the onset of melting, the surface energy of the smaller cluster is larger than the surface energy of the larger clusters, while at temperatures above the permanent and complete melting the order is reversed as shown in Fig. 3.

Naturally, also the crystal surface morphology is a strong function of temperature, as shown in Fig. 4 and 5 for the Au_{561} and Au_{3871} icosahedral clusters, respectively. It can be seen that the facets on the surface of the icosahedral gold clusters soften, but do not pre-melt below the melting temperature. This softening is due to the increasing mobility of vertex and edge atoms with temperature.[85] As a result, the average shape of the cluster is nearly spherical at the onset of melting.

We also performed a bond-angle analysis to gain insight into the possible change in the crystal structure upon heating. This analysis demonstrates that in both Au_{561} and Au_{3871} the local coordination of the atoms in the particles changes quite siginificantly with temperature. Specifically, at 100 K, the Au_{3871} cluster contains 43.4% atoms in fcc configuration and 30.7% atoms in hcp configuration. At 1300 K, however, these numbers drop to only 1.2% and 14.6% for fcc and hcp, respectively. Moreover, there are no amorphous core at 100 K, increasing to 11.4% at 1300 K. A similar result is also found for the Au_{561} cluster, *i.e.*, the number of atoms in fcc and hcp coordination decreases with temperature, while the fraction of amorphous core atoms increases.

There are different methods for analyzing nanocluster melting, including *e.g.* calculating a suitable order parameter such as the Lindemann index[86] calculating the free energies of solid and liquid states employing standard thermodynamic integration, or calculating the radial distribution function (RDF).[87,88]

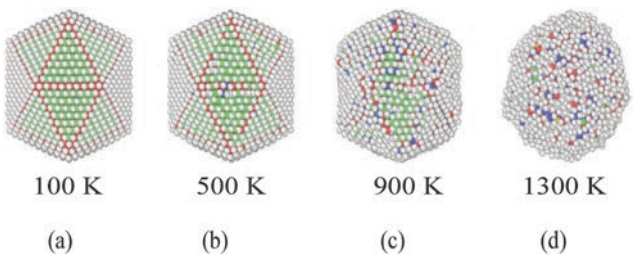

Fig. 5 Icosahedral structure of the Au_{3871} cluster at (a) T = 100 K, (b) T = 500 K, (c) T = 900 K and (d) T = 1300 K. Color coding is the same as in Fig. 4.

Here we consider the RDF along with the caloric curve to analyse the melting behavior of the considered clusters, similar to earlier MD studies on Au nanocluster melting.[78]

Fig. 6 shows the variation of RDF with temperature. While the crystallinity can be clearly seen at 100 °C for both Au_{3871} (a) and Au_{561} (b), the sharp peaks indicative of a crystalline structure dissappear with increasing temperature. At a temperature of around 900 °C, the peaks spread out, indicative of melting.

This corresponds to the calculated caloric curves as shown in Fig. 7. A sharp increase in energy can be seen at 800 K and 900 K for the smaller (a) and larger (b) clusters, respectively, typical for signaling the onset of melting of the clusters.

3.2. Surface energy of cuboctahedral, truncated octahedral and decahedral gold nanoclusters

Similar to the results shown above for the icosahedral clusters, the surface energies of cuboctahedral, truncated octahedral and decahedral clusters at 0 K are found to decrease with increasing cluster size as shown in Fig. 8. For a given number of atoms, cuboctahedral clusters show a slightly higher surface energy than the icosahedra in the case of the smaller clusters (Au_{309} and Au_{923}), while for bigger clusters (Au_{2057} and Au_{3871}), the decahedra are found to have a slightly lower surface energy. This is shown in Fig. 9. This effect is caused by the stability of the clusters as discussed above. Indeed, for smaller clusters icosahedra are more stable while for larger clusters decahedra are most stable. This result is in line with earlier literature reports.[31]

As shown in Fig. 10, we also compared our surface energy calculations to calculations employing the Modified Embedded Atom Method (MEAM) and calculations at the tight-binding (TB) level, using the potential developed by Cleri and Rosato.[89] The latter potential was previously used to describe the behavior of a number of thermodynamic characteristics of Au and other fcc metals.[90] While the MEAM potential gives a slightly higher value for the surface energy, and the TB potential gives a lower surface energy, the observed trend in the three calculations confirms the decreasing surface energy with increasing cluster size.

3.3. Displacement and strain calculation

As mentioned above, strain and strain energy are also important descriptors for nanoclusters, in particular in relation to their reactivity. We therefore also calculate the strain, strain energies, and atomic displacements in icosahedral, cuboctahedral and truncated octahedral clusters as a function of cluster size. Strain energies are calculated using eqn (2)

$$E_{\text{strain}} = E_{\text{unrelaxed}} - E_{\text{relaxed}} \quad (2)$$

where E_{relaxed} is the potential energy of the cluster after minimization and $E_{\text{unrelaxed}}$ is the potential energy of the cluster with all atoms in their ideal lattice positions. The minimum energy structure (*i.e.* the relaxed structure) is considered as the reference structure. We calculate the strain using eqn (3)

$$\varepsilon = \frac{\Delta D}{D} \quad (3)$$

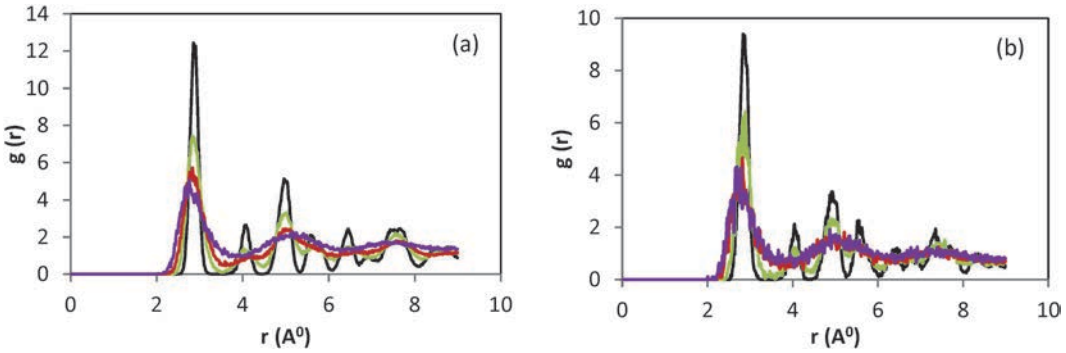

Fig. 6 The radial distribution function of the icosahedral clusters Au_{3871} (a) and Au_{561} (b) at 100 (black), 500 (green), 900 (red) and 1300 K (purple).

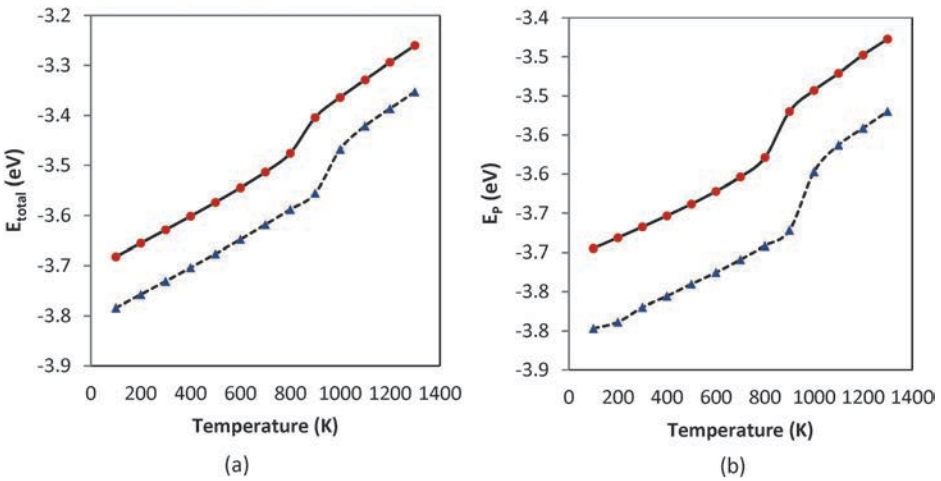

Fig. 7 (a) Caloric curve for the icosahedral clusters Au_{561} (red circles) and Au_{3871} (blue triangles). (b) Potential energy curves for the icosahedral clusters Au_{561} (red circles) and Au_{3871} (blue triangles) as a function of temperature in the range 0–1300 K.

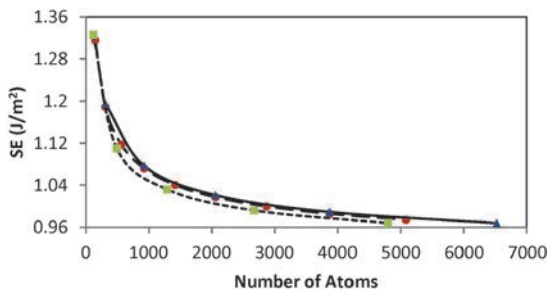

Fig. 8 Calculated surface energies for different cuboctahedra (blue triangles), truncated octahedra (green squares) and decahedra (red circles).

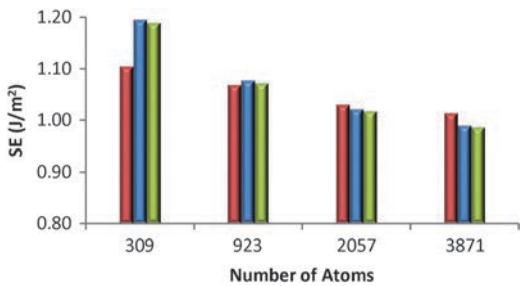

Fig. 9 Calculated surface energies for icosahedral, cuboctahedral and decahedral clusters containing the same number of atoms. Red, blue and green bars indicate icosahedral, cuboctahedral and decahedral structures, respectively.

where D is the diameter of the cluster in its minimum energy structure and ΔD is the change in this dimension upon positioning the atoms in their ideal bulk positions.

Fig. 11 shows the strain energy per atom for icosahedral, cuboctahedral, truncated octahedral and decahedral clusters as a function of size at 0 K. With increasing size, a continuous increase in strain energy is observed for icosahedral clusters, while a continuous decrease in strain energy (*i.e.*, towards zero) is observed for cuboctahedral and truncated octahedral clusters. Therefore, perfect icosahedra become increasingly less stable with increasing size due to the elastic distortion associated with their five-fold symmetry. Cuboctahedra and truncated octahedra, on the other hand, increasingly resemble the fcc bulk structure with increasing size. Moreover, with increasing size, the importance of the surface energy (which is higher for the cuboctahedral clusters, due to the presence of the {100} facets) decreases, since the fraction of surface atoms decreases with increasing cluster size. Therefore, the smallest clusters assume the icosahedral configuration while larger clusters will adopt the fcc configuration.

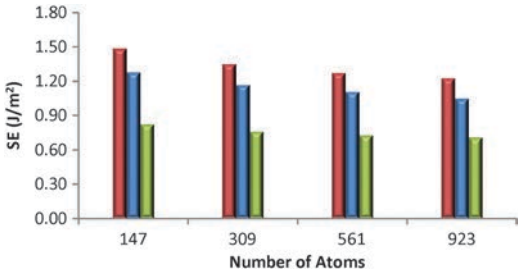

Fig. 10 A comparison between different potentials for surface energy calculation of icosahedral clusters. Red, blue and green bars indicate MEAM, EAM and TB_SMA potentials, respectively.

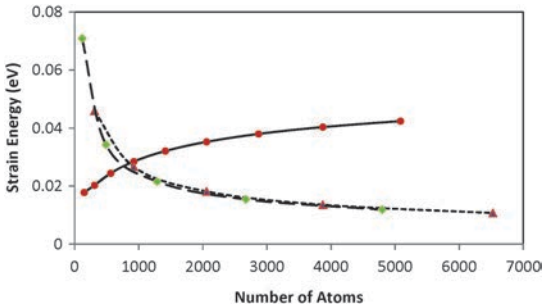

Fig. 11 Strain energy calculations for different icosahedral (red circles), cuboctahedral (blue triangles) and truncated octahedral (green squares) Au clusters.

Fig. 12 shows the calculated volumetric strain and atomic displacements for the icosahedral Au_{309} nanocluster (NC). The colors represent the strain values. Interestingly, it can be seen that atoms at edges and corners relax with inward displacements while terrace atoms are displaced outwards. Similarly, shorter and stronger bonds for under-coordinated atoms in comparison to those between fully coordinated atoms in the bulk have been reported,[91,92] which is in line with our observation of contraction of vertex atoms compared to the expansion of face atoms in nanoclusters. Moreover, for smaller clusters there are more under-coordinated atoms (and hence stronger bonds) and therefore a higher surface energy compared to larger clusters at 0 K.

Thus, the clusters are observed to assume a round shape upon relaxation, which is in agreement with experimental

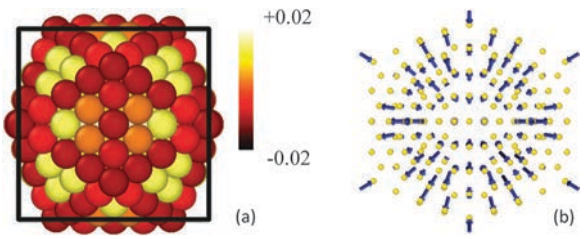

Fig. 12 (a) Calculated volumetric strain for the icosahedral Au_{309} cluster. While atoms in the center of the faces move outwards ("expand") as indicated by the yellow colour, corner and edge atoms move inwards ("contract") as indicated by the dark red colour. (b) Calculated displacement vectors, showing an inward displacement of vertex atoms and an outward displacement of face atoms.

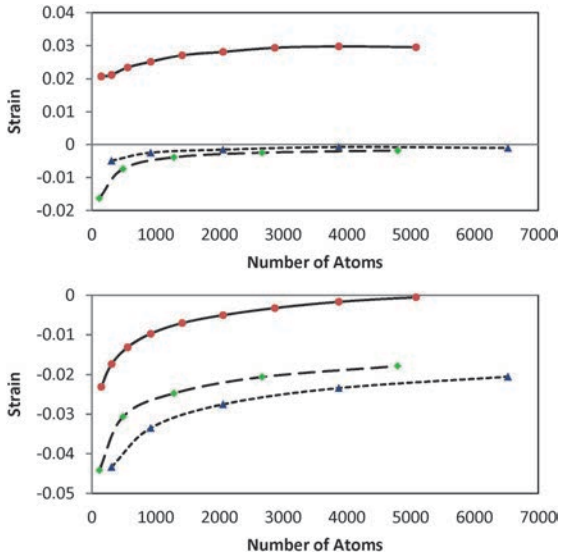

Fig. 13 Strain calculations based on face-centered atoms (top panel) and vertex-atoms (bottom panel) for icosahedral (red circles), cuboctahedral (blue triangles) and truncated octahedral (green squares) Au clusters, as a function of size.

observations.[58,93] Moreover, edges and corners are found to relax with larger displacements, corresponding to a larger lattice strain, compared with the center position. Again, this observation is consistent with experimental results.[58,93]

Finally, the strain also strongly depends on the cluster size and increases with increasing size. This is shown in Fig. 13, calculated for both face-to-face and vertex-to-vertex distances. Note that since the vertices of icosahedra are displaced inwards upon relaxation, negative strain values are obtained in this case, while the face atoms displace slightly outwards upon relaxation, such that in this case positive strain values are obtained. It can be seen that the icosahedra show an increasing expansion in the direction normal to the faces with increasing size, and a vanishing contraction along the direction of the connection line between any two opposite vertex atoms. In cuboctahedral and truncated octahedral clusters, in contrast, face atoms and vertex atoms both tend to attain zero contraction upon increasing the cluster size.

4. Conclusions

We have calculated surface energies, atomic displacements, strain and strain energies for icosahedral, cuboctahedral, truncated octahedral and decahedral Au nanoclusters of different sizes, which is of importance in characterizing these clusters and understanding their physico-chemical properties. The results show that the surface energy decreases with cluster size at 0 K but increases at higher temperatures after melting. Typical melting point curves as a function of cluster size are also calculated, demonstrating the Gibbs–Thomson effect. Atomic displacements are found to strongly depend on the cluster size, showing an increase in the absolute value with increasing size. Also the strain is found to increase with increasing cluster size, thus tends to

become zero for negative strain and increases in the absolute value for positive strain. While for icosahedral clusters the strain energy is found to increase with increasing cluster size, the opposite trend is observed for both cuboctahedral and truncated octahedral clusters. Our study shows that all investigated properties are strongly dependent on the cluster size. These results are of importance for understanding the size-dependent surface properties and processes of Au nanoclusters.

Acknowledgements

The authors acknowledge financial support from the Research Foundation Flanders (FWO), grant G021814N. This work was carried out in part using the Turing HPC infrastructure at the CalcUA core facility of the Universiteit Antwerpen (UA), a division of the Flemish Supercomputer Center VSC, funded by the Hercules Foundation, the Flemish Government (department EWI) and the UA.

References

1 H. Häkkinen, S. Abbet, A. Sanchez, U. Heiz and U. Landman, Structural, Electronic, and Impurity-Doping Effects in Nanoscale Chemistry: Supported Gold Nanoclusters, *Angew. Chem.*, 2003, **42**(11), 1297–1300.

2 B. Medasani, Y. H. Park and I. Vasiliev, Theoretical study of the surface energy, stress, and lattice contraction of silver nanoparticles, *Phys. Rev. B: Condens. Matter Mater. Phys.*, 2007, **75**, 235436.

3 A. Puzder, A. J. Williamson, F. A. Reboredo and G. Galli, Structural Stability and Optical Properties of Nanomaterials with Reconstructed Surfaces, *Phys. Rev. Lett.*, 2003, **91**(15), 157405.

4 J. Zheng, Z. Chen and Z. Liu, Atomic Force Microscopy-Based Nanolithography on Silicon Using Colloidal Au Nanoparticles as a Nanooxidation Mask, *Langmuir*, 2000, **16**(24), 9673–9676.

5 F. Seker, P. R. L. Malenfant, M. Larsen, A. Alizadeh, K. Conway and A. M. Kulkarni, *et al.*, On-Demand Control of Optoelectronic Coupling in Gold Nanoparticle Arrays, *Adv. Mater.*, 2005, **17**(16), 1941–1945.

6 S. A. Maier, P. G. kik, H. A. Atwater, S. Meltzer, E. Harel and B. E. Koel, *et al.*, Local detection of electromagnetic energy transport below the diffraction limit in metal nanoparticle plasmon waveguides, *Nat. Mater.*, 2003, **2**, 229–232.

7 B. Yoon, H. Hakkinen, U. Landman, A. S. Worz, J. M. Antonietti and S. Abbet, *et al.*, Charging Effects on Bonding and Catalyzed Oxidation of CO on Au_8 Clusters on MgO, *Science*, 2005, **307**, 403–407.

8 M. Valden, X. Lai and D. W. Goodman, Onset of Catalytic Activity of Gold Clusters on Titania with the Appearance of Nonmetallic Properties, *Science*, 1998, **281**, 1647–1650.

9 B. Hvolbaek, T. V. W. Janssens, B. S. Clausen, H. Falsig, C. H. Christensen and J. K. Norskov, Catalytic Activity of Au Nanoparticles, *Nano Today*, 2007, **2**, 14–18.

10 I. H. El-Sayed, X. Huang and M. A. El-Sayed, Surface Plasmon Resonance Scattering and Absorption of anti-EGFR Antibody Conjugated Gold Nanoparticles in Cancer Diagnostics: Applications in Oral Cancer, *Nano Lett.*, 2005, **5**(5), 829–834.

11 G. Ouyang, C. X. Wang and G. W. Yang, Surface Energy of Nanostructural Materials with Negative Curvature and Related Size Effects, *Chem. Rev.*, 2009, **109**(9), 4221–4247.

12 H. Akbarzadeh and F. Taherkhani, Cluster size dependence of surface energy of Ni nanoclusters: a molecular dynamics study, *Chem. Phys. Lett.*, 2013, **558**, 57–61.

13 D. Holec, P. Dumitraschkewitz, F. D. Fischer and D. Vollath, *Size-dependent surface energies of Au nanoparticles*, 2015, http://arxiv.org/pdf/1412.7195v3.pdf.

14 M. Grzelczak, J. Perez-Juste, P. Mulvaney and M. Liz-Marzan, Shape control in gold nanoparticle synthesis, *Chem. Soc. Rev.*, 2008, **37**(9), 1783–1791.

15 Y. Chen, X. Gu, C. G. Nie, Z. Y. Jiang, Z. X. Xie and C. J. Lin, Shape controlled growth of gold nanoparticles by a solution synthesis, *Chem. Commun.*, 2005, 4181–4183.

16 E. C. Neyts and K. Ostrikov, Nanoscale Thermodynamic Aspects of Plasma Catalysis, *Catal. Today*, 2015, **256**, 23–28.

17 F. Klasovsky and P. Claus, Metal Nanoclusters in Catalysis: Effects of Nanoparticle Size, Shape and Structure, in *Metal Nanoclusters in Catalysis and Materials Science: The Issue of Size Control*, ed. B. Corain, G. Schmid and N. Toshima, Elsevier, Amsterdam, 2008, ch. 8.

18 K. Kendall, N. Mcn.Alford and J. D. Birchall, A new method for measuring the surface energy of solids, *Nature*, 1986, **325**, 794–796.

19 K. K. Nanda, A. Maisels and F. E. Kruis, Surface Tension and Sintering of Free Gold Nanoparticles, *Phys. Chem. C*, 2008, **112**(35), 13488–13491.

20 K. K. Nanda, A. Maisels, F. E. Kruis, H. Fissan and S. Stappert, Higher surface energy of free nanoparticles, *Phys. Rev. Lett.*, 2003, **91**, 106102.

21 H. M. Lu and Q. Jiang, Comment on ''Higher Surface Energy of Free Nanoparticles'', *Phys. Rev. Lett.*, 2004, **92**(17), 179601.

22 W. R. Tyson and W. A. Miller, Surface free Energies of Solid Metals. Estimation from Liquid Surface Tension Measurements, *Surf. Sci.*, 1977, **62**, 267–276.

23 J. M. Blakely, *Introduction to the properties of crystal surfaces*, Pergamon, New York, 1973.

24 H. Mykura, *Solid surfaces and interfaces*, Dover Publications, New York, 1966.

25 R. G. Linford, Surface energy of solids, *Chem. Soc. Rev.*, 1972, **1**(4), 445–464.

26 F. R. De Boer, R. Boom, W. C. M. Mattens, A. R. Miedema, A. K. Niessen and A. K. Niessen, *Cohession in Metals Amsterdam*, North Holland, 1988.

27 W. R. Tyson, Surface energies of solid metals, *Can. Metall. Q.*, 1975, **14**(4), 307–314.

28 L. Vitos, A. V. Ruban, H. L. Skriver and J. Kollar, The surface energy of metals, *Surf. Sci.*, 1998, **411**, 186–202.

29 W. P. Halperin, Quantum size effects in metal particles, *Rev. Mod. Phys.*, 1966, **58**, 533.

30 M. A. El-Sayed, Some Interesting Properties of Metals Confined in Time and Nanometer Space of Different Shapes, *Acc. Chem. Res.*, 2001, **34**(4), 257.
31 Z. Y. Li, N. P. Young, M. D. Vece, S. Palomba, R. E. Palmer and A. L. Bleloch, *et al.*, Three-dimensional atomic-scale structure of size-selected gold nanoclusters, *Nature*, 2008, **451**, 46–49.
32 H. S. Lim and C. K. Ong, Stability of face-centered cubic and icosahedral lead clusters, *Surf. Sci.*, 1992, **269/270**, 1109–1115.
33 S. Ino, Stability of Multiply-Twinned Particles, *J. Phys. Soc. Jpn.*, 1969, **27**, 941–953.
34 Y. Wang, S. Teitel and C. Dellago, Melting of icosahedral gold nanoclusters from molecular dynamics simulations, *J. Chem. Phys.*, 2005, **122**(21), 214722.
35 P. Carnevali, F. Ercolessi and E. Tosatti, Melting and nonmelting behavior of the Au(111) surface, *Phys. Rev. B: Condens. Matter Mater. Phys.*, 1987, **36**(12), 6701–6704.
36 K. D. Stock and B. Grosser, Topography and Surface Melt on Spherical Gold Crystals after Purification by a Pre-melt in Air, *J. Cryst. Growth*, 1980, **50**(2), 485–490.
37 R. Henry, Morphology of supported nanoparticles, *Prog. Surf. Sci.*, 2005, **80**(3–4), 92–116.
38 G. Z. Wulff, Kristallogr, *Mineral*, 1901, **34**, 449–530.
39 M. J. Walsh, S. J. Barrow, W. Tong, A. M. Funston and J. Etheridge, Symmetry Breaking and Silver in Gold Nanorod Growth, *ACS Nano*, 2015, **9**(1), 715–724.
40 A. S. Barnard, X. M. Lin and L. A. Curtiss, Equilibrium Morphology of Face-Centered Cubic Gold Nanoparticles >3 nm and the Shape, *J. Phys. Chem. B*, 2005, **109**, 24465–24472.
41 J. L. Aargon, Transition from multiply twinned icosahedral to cuboctahedral symmetry in particles of arbitrary size, *Chem. Phys. Lett.*, 1994, **226**, 263–267.
42 C. L. Kuo and P. Clancy, Melting and Freezing Characteristics and Structural Properties of Supported and Unsupported Gold Nanoclusters, *Phys. Chem. B*, 2005, **109**(28), 13743–13754.
43 A. V. Myshlyavtsev and P. V. Stishenko, Relative stability of icosahedral and cuboctahedral metallic nanoparticles, *Adsorption*, 2013, **19**, 795–801.
44 G. Treglia, I. Meunier, C. Mottet, J. M. Roussel, A. Saul and A. Senhaji, *et al.*, Atomistic modeling of bimetallic surfaces, in *Quasicrystals Current Topics*, ed. A. Sadoc, E. Belin-Ferre, C. Berger and M. Quiquandon, Word Scientific, Singapore, 2000, p. 243.
45 F. Taherkhani, H. Akbarzadeh and H. Rezania, Chemical ordering effect on melting temperature, surface energy of copper–gold bimetallic nanocluster, *J. Alloys Compd.*, 2014, **617**, 746–750.
46 B. Medasani and I. Vasiliev, Computational study of the surface properties of aluminum nanoparticles, *Surf. Sci.*, 2009, **603**, 2042–2046.
47 E. K. Yildirim, M. Atis and Z. B. Guvenc, Molecular dynamics simulation of melting behaviour of small gold clusters: AuN (N = 12–14), *Phys. Scr.*, 2007, **75**, 111–118.
48 Y. G. Chushak and L. S. Bartell Melting, Freezing of Gold Nanoclusters, *J. Phys. Chem. B*, 2001, **105**, 11605–11614.
49 C. L. Cleveland, W. D. Luedtke and U. Landman, Melting of Gold Clusters, *Phys. Rev. B: Condens. Matter Mater. Phys.*, 1991, **60**(7), 5065–5077.
50 C. L. Cleveland, W. D. Luedtke and U. Landman, Melting of Gold Clusters: Icosahedral Precursors, *Phys. Rev. Lett.*, 1998, **81**(10), 2036–2039.
51 L. J. Lewis, P. Jensen and J. L. Barrat, Melting, freezing, and coalescence of gold nanoclusters, *Phys. Rev. B: Condens. Matter Mater. Phys.*, 1997, **56**(4), 2248–2257.
52 J. C. R. Gomez and L. Rincon, Melting of intermediate-sized gold nanoclusters, *Rev. Mex. Fis.*, 2007, **53**(7), 208–211.
53 S. J. Zhao, S. Q. Wang, Z. Q. Yang and H. Q. Ye, Coalescence of three silver nanoclusters: a molecular dynamics study, *J. Phys.: Condens. Matter*, 2001, **13**, 8061–8069.
54 L. Wang, Y. Zhang, X. Bian and Y. Chen, Melting of Cu nanoclusters by molecular dynamics simulation, *Phys. Lett. A*, 2003, **310**, 197–202.
55 E. C. Neyts and A. Bogaerts, Numerical Study of the Size-Dependent Melting Mechanisms of Nickel Nanoclusters, *J. Phys. Chem. C*, 2009, **113**, 2771–2776.
56 S. K. R. S. Sankaranarayanan, V. R. Bhethanabotla and B. Joseph, Molecular dynamics simulation study of the melting of Pd-Pt nanoclusters, *Phys. Rev. B: Condens. Matter Mater. Phys.*, 2005, **71**, 195415.
57 M. H. Ghatee and K. Shekoohi, Melting profile of cesium metal nanoclusters by molecular dynamics simulation, *Fluid Phase Equilib.*, 2012, **327**, 14–21.
58 G. Ouyang, W. G. Zhu, C. Q. Sun, Z. M. Zhu and S. Z. Liao, Atomistic origin of lattice strain on stiffness of nanoparticles, *Phys. Chem. Chem. Phys.*, 2010, **12**, 1543–1549.
59 M. S. Daw and M. I. Baskes, Semiempirical, Quantum Mechanical Calculation of Hydrogen Embrittlement in Metals, *Phys. Rev. Lett.*, 1983, **50**(17), 1285–1288.
60 M. S. Daw and M. I. Baskes, Embedded-atom method: derivation and application to impurities, surfaces, and other defects in metals, *Phys. Rev. B: Condens. Matter Mater. Phys.*, 1984, **29**(12), 6443–6453.
61 S. Plimpton, Fast Parallel Algorithms for Short-Range Molecular Dynamics, *J. Comp. Physiol.*, 1995, **117**, 1–19.
62 http://lammps.sandia.gov/.
63 R. E. Palmer, R. L. Johnston and J. Wilcoxon, *Metal Nanoparticles and Nanoalloys Amsterdam*, Elsevier Ltd., 2012.
64 P. Pyykko, Structural properties: magic nanoclusters of gold, *Nat. Nanotechnol.*, 2007, **2**, 273–274.
65 H. Li, L. Li, A. Pedersen, Y. Gao, N. Khetrapal and H. Jonsson, *et al.*, Magic-Number Gold Nanoclusters with Diameters from 1 to 3.5 nm: Relative Stability and Catalytic Activity for Co Oxidation, *Nano Lett.*, 2014, **15**, 682–688.
66 S. Luo, *Discussion on the origin of magic numbers in clusters*, Ohio State University, Department of Chemical and Biomolecular Engineering, 2014.
67 I. Stich, R. Car, M. Parrinello and S. Baroni, Conjugate gradient minimization of the energy functional: a new method for electronic structure calculation, *Phys. Rev. B: Condens. Matter Mater. Phys.*, 1989, **39**(8), 4997–5004.

68 A. K. Rappe and C. J. Casewit, *Molecular Mechanics across Chemistry Sausalito*, University Science Books, 1997.
69 W. G. Hoover, Canonical dynamics: equilibrium phase-space distributions, *Phys. Rev. A: At., Mol., Opt. Phys.*, 1985, **31**(3), 1695–1697.
70 C. B. Barber, D. P. Dobkin and H. Huhdanpaa, The Quickhull Algorithm for Convex Hulls, *ACM Transactions on Mathematical Software*, 1996, **22**(4), 469–483.
71 Qhull: computational code for calculating surface area, volume *etc.*, online, Available from: http://www.qhull.org.
72 G. J. Ackland and A. P. Jones, Applications of local crystal structure measures in experiment and simulation, *Phys. Rev. B: Condens. Matter Mater. Phys.*, 2006, **73**(5), 054104.
73 A. Stukowski, Visualization and analysis of atomistic simulation data with OVITO–the open visualization tool, *Modell. Simul. Mater. Sci. Eng.*, 2010, **18**, 015012.
74 A. Stukowski, Ovito: scientific visualization and analysis software for atomistic simulation data, online, available from: http://ovito.org/.
75 N. E. Singh-Miller and N. Marzari, Surface energies, work functions, and surface relaxations of low index metallic surfaces from first-priciples, *Phys. Rev. B: Condens. Matter Mater. Phys.*, 2009, **80**, 235407.
76 N. Almora-Barrios, G. Novell-Leruth, P. Whiting, L. M. Liz-Marzan and N. Lopez, Theoratical Description of the Rold of Halides, Silver, and Surfactants on the Structure of Gold Nanorods, *Nano Lett.*, 2014, **14**, 871–875.
77 Z. Crljen, P. Lazic, D. Sokceviv and R. Brako, Relaxation and reconstruction on 111… surfaces of Au, Pt, and Cu, *Phys. Rev. B: Condens. Matter Mater. Phys.*, 2003, **68**, 195411.
78 J. A. Keith, D. Fantauzzi and T. Jacob, Reactive forcefield for simulating gold surfaces and nanoparticles, *Phys. Rev. B: Condens. Matter Mater. Phys.*, 2010, **81**, 235404.
79 E. Ricci and R. Novakovic, Wetting and Surface Tension Measurements on Gold Alloys, *Gold Bull.*, 2001, **34**(2), 41–49.
80 C. W. Mays, J. S. Vermaak and D. Kuhlmann-Wilsdorf, On Surface Stress and Surface Tension II. Determination of the Surface Stress of Gold, *Surf. Sci.*, 1968, **12**, 134–140.
81 J. Diao, K. Gall and M. L. Dunn, Surface-stress-induced phase transformation in metal nanowires, *Nat. Mater.*, 2003, **2**, 656–660.
82 P. Brault and E. C. Neyts, Molecular dynamics simulations of supported metal nanocatalyst formation by plasma sputtering, *Catal. Today*, 2015, **256**, 3–12.
83 Y. Engelmann, A. Bogaerts and E. C. Neyts, Thermodynamics at the nanoscale: phase diagrams of nickel-carbon nanoclusters and equilibrium constants for phase transitions, *Nanoscale*, 2014, **6**, 11981.
84 Y. Shibuta and T. Suzuki, Melting and nucleation of iron nanoparticles: a molecular dynamics study, *Chem. Phys. Lett.*, 2007, **445**, 265–270.
85 Y. Wang, S. Teitel and C. Dellago, Melting and equilibrium shape of icosahedral gold nanoparticles, *Chem. Phys. Lett.*, 2004, **394**(4–6), 257–261.
86 F. A. Lindemann, *Phys. Z.*, 1910, **11**, 609.
87 Z. Qiao, H. Feng and J. Zhou, Molecular dynamics simulations on the melting of gold nanoparticles, *Phase Transitions*, 2014, **87**(1), 59–70.
88 A. R. Leach, *Molecular Modelling: Principles and Applications Essex*, Pearson Education Limited, 2001.
89 F. Cleri and V. Rosato, Tight-binding potentials for transition metals and alloys, *Phys. Rev. B: Condens. Matter Mater. Phys.*, 1993, **48**(1), 22–33.
90 Z. V. Goloven'ko, Y. Y. Gafner, S. L. Gafner and L. V. Redel, Thermal Stability of Structure in Small Gold Clusters, *Phys. Met. Metallogr.*, 2013, **114**(12), 1038–1044.
91 X. Liu, X. Zhang, M. Bo, L. Li, H. Tian and Y. Nie, *et al.*, Coordination-Resolved Electron Spectrometrics, *Chem. Rev.*, 2015, **115**(14), 6746–6810.
92 C. Q. Sun, Size dependence of nanostructures: impact of bond order deficiency, *Prog. Solid State Chem.*, 2007, **35**(1), 1–159.
93 M. V. Rastei, B. Heinrich, L. Limot, P. A. Lgnatiev, V. S. Stepanyuk and P. Bruno, *et al.*, Size-Dependent Surface States of Strained Cobalt Nanoislands on Cu(111), *Phys. Rev. Lett.*, 2007, **99**, 246102.

